ACS NANO

www.acsnano.org

ARTICLE

PEGylated Polyester Nanoparticles Trigger Adverse Events in a Large Animal Model of Trauma and in Naïve Animals: Understanding Cytokine and Cellular Correlations with These Events

Nuzhat Maisha, Chhaya Kulkarni, Narendra Pandala, Rose Zilberberg, Leasha Schaub, Leslie Neidert, Jacob Glaser, Jeremy Cannon, Vandana Janeja, and Erin B. Lavik*

Cite This: *ACS Nano* 2022, 16, 10566–10580

Read Online

ACCESS | Metrics & More | Article Recommendations | Supporting Information

ABSTRACT: Intravenously infusible nanoparticles to control bleeding have shown promise in rodents, but translation into preclinical models has been challenging as many of these nanoparticle approaches have resulted in infusion responses and adverse outcomes in large animal trauma models. We developed a hemostatic nanoparticle technology that was screened to avoid one component of the infusion response: complement activation. We administered these hemostatic nanoparticles, control nanoparticles, or saline volume controls in a porcine polytrauma model. While the hemostatic nanoparticles promoted clotting as marked by a decrease in prothrombin time and both the hemostatic nanoparticles and controls did not active complement, in a subset of the animals, hard thrombi were found in uninjured tissues in both the hemostatic and control nanoparticle groups. Using data science methods that allow one to work across heterogeneous data sets, we found that the presence of these thrombi correlated with changes in IL-6, INF-alpha, lymphocytes, and neutrophils. While these findings might suggest that this formulation would not be a safe one for translation for trauma, they provide guidance for developing screening tools to make nanoparticle formulations in the complex milieux of trauma as well as for therapeutic interventions more broadly. This is important as we look to translate intravenously administered nanoparticle formulations for therapies, particularly considering the vascular changes seen in a subset of patients following COVID-19. We need to understand adverse events like thrombi more completely and screen for these events early to make nanomaterials as safe and effective as possible.

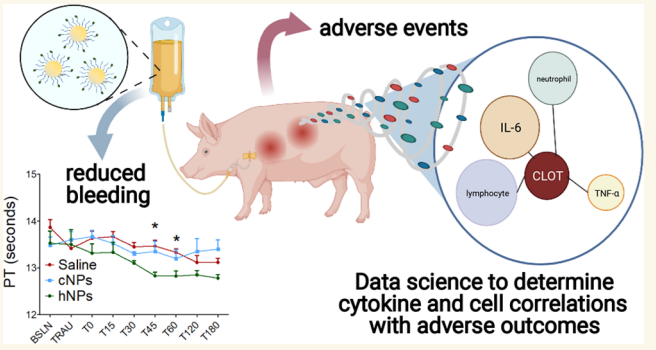

KEYWORDS: *hemorrhage, inflammation, IL-6, neutrophils, lymphocytes, TNF-alpha, hemostasis*

Traumatic injury is the leading cause of death in men, women, and children between the ages of 1 and 46 worldwide,[1] and blood loss is the primary cause of death at acute time points postinjury in both civilian[2] and battlefield trauma.[3] While rapid intervention to achieve hemostasis is imperative to minimize mortality associated with severe trauma,[4,5] pressure dressings and absorbent topical agents are currently the only hemostats available for field use. We need therapies that can be administered in the field to control bleeding for noncompressible junctional and torso internal injuries.[6] To address this need, many groups have developed intravenously infusible nanomaterials.[7−11]

While many agents have shown promise in small animal models, translating the work to large animal models has proven exceptionally difficult in great part because of complement activation to intravenously infused agents, including both cell-

Received: February 25, 2022
Accepted: July 11, 2022
Published: July 13, 2022

https://doi.org/10.1021/acsnano.2c01993
ACS Nano 2022, 16, 10566−10580

derived and nanomaterial systems.[12−16] Complement activation is extremely rapid and triggers vasodilation, which significantly hinders the hemostatic effect of any technology. Unfortunately, approximately 10% of humans exhibit the same significant response during infusions of the liposomal formulation of doxorubicin (DOXIL)[17] as well as infusions of biologics.[18] These complement responses have been observed by us and others and are particularly challenging in the context of infusible treatments for trauma given the urgency and time-sensitive nature of hemostatic treatments. Slow infusions can reduce infusion responses,[19,20] but a slow infusion rate would risk unmitigated hemorrhage before the hemostatic agent is delivered in patients with major hemorrhage.

We have been developing and testing hemostatic nanoparticles that can be infused intravenously to stop bleeding and improve survival in several of rodent models of trauma.[21−25] However, in a porcine model of trauma, we saw that these particles triggered complement activation and vasodilation, leading to a rapid drop in blood pressure, blood gas changes, and, ultimately, increased bleeding.[26] We found that by modulating the charge on these hemostatic nanoparticles, we could reduce this complement response and halt bleeding in the large animal model, but at the highest doses, we still saw exacerbation of bleeding.[26] This motivated us to develop a screening assay for complement activation with nanoparticles that was more sensitive than the ones most commonly described in the field.[27] Using this assay, we identified a hemostatic nanoparticle formulation with two molecular weights of poly(ethylene oxide) (PEG) that led to no measurable complement activation in vitro.[28] On this basis, we sought to determine the safety and efficacy of these hemostatic nanoparticles in a large animal model of trauma, a critical step in translating nanoparticles for trauma applications.

In this work, we tested these hemostatic nanoparticles, control nanoparticles, or saline in a porcine liver injury model and assessed their impact on bleeding, survival, and immune responses following administration. We also tested the nanoparticles and controls in naïve uninjured animals to parse out the impact of the nanoparticles from the trauma as trauma independently leads to significant changes in inflammatory markers. We applied data science methods to look for correlations between outcomes and biological parameters, including physiological data, cytokines, and immune cells, to understand the impact of the infusion of nanoparticles on immune responses beyond complement responses. This work provides a foundation for understanding the complex role of infusion responses and approaches to mitigate their effect.

RESULTS AND DISCUSSION

Nanoparticle Design and Characterization. On the basis of our previous work screening nanoparticles, we used poly(lactic acid) (PLA)−PEG nanoparticles consisting of a blend of PLA−PEG with a PEG molecular weight of 5000 Da (75 wt %) and a PLA−PEG with a PEG molecular weight of 3400 Da (25 wt %) as the platform for the nanoparticles in this study. We have previously shown that this blend is highly PEGylated (92%)[28] and leads to no measurable complement activation in vitro, as marked by changes in C5a.[28] To make these nanoparticles hemostatic, we conjugated the GRGDS peptide to the PLA−PEG nanoparticles using EDC/NHS chemistry following our previous work.[21] The GRGDS peptide binds with the glycoprotein IIb/IIIa receptor on activated platelets, and this binding can be inhibited by blocking the glycoprotein IIb/IIIa receptor which, in turn, blocks the hemostatic capacity of the PLA−PEG−GRGDS system.[21] Therefore, we have two nanoparticles in this work: control nanoparticles based on PLA−PEG and hemostatic nanoparticles based on PLA−PEG with GRGDS conjugated following the nanoparticle fabrication procedure.

Each batch of nanoparticles was characterized for size, ζ-potential, and peptide content. The average values across batches are in Figure 1, and the detailed values for each batch are in Supplementary Tables 1 and 2.

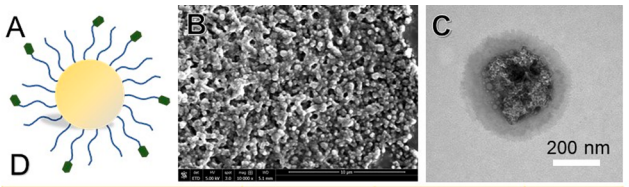

	Diameter (nm)	Zeta Potential (mV)	peptide content (%)
Control nanoparticles	372±18	-15.5±0.9	
Hemostatic nanoparticles	441±25	-13.6±0.8	6.75

Figure 1. Nanoparticle characterization for large animal studies. (A) Schematic of the PLA−PEG based nanoparticles functionalized with GRGDS for the studies. (B) SEM micrograph of PLA−PEG nanoparticles. (C) TEM micrograph of PLA−PEG nanoparticle showing the PEG corona. (D) Table of properties of PLA−PEG control and PLA−PEG-GRGDS hemostatic nanoparticles.

The average hydrodynamic diameter and ζ-potential in a 10 mM KCl solution of each batch were determined using dynamic light scattering (DLS). The amount of peptide was quantified using the orthopthaladehyde (OPA) assay. The presence of the peptide increases the hydrodynamic diameter of the hNPs versus the cNPs, thus impacting the DLS values slightly, as has been seen previously.[21] However, scanning electron microscopy (SEM) analysis of both the control and hemostatic nanoparticles showed no differences in the size of the core (Figure 1B). Transmission electron microscopy (TEM) of nanoparticles showed what may be the PEG corona of the nanoparticles (Figure 1C). We have seen this previously,[28] but only at the highest degrees of PEGylation.

While the nanoparticle formulation was chosen because it showed no measurable change in complement in vitro,[28] we confirmed the lack of change in each batch before administration in vivo (Supplementary Figure 1). It should be noted that there is some batch-to-batch variability in the size of the nanoparticles (Supplementary Table 1.) However, we did not see an impact of the size variation on complement activation or in vivo outcomes, as described in more detail in the following.

Administration of the Nanoparticles in a Porcine Model of Trauma. All animal procedures were approved by the 711th HPW/RHD JBSA-Fort Sam Houston Institutional Animal Care and Use Committee (IACUC) in compliance with all applicable Federal regulations governing the protection of animals in research.

Following sedation, animals were intubated, and sedation was maintained on 1−3% isoflurane. A midline laparotomy was performed to expose the spleen and liver. A splenectomy was performed. Next 30% total blood was collected from a

https://doi.org/10.1021/acsnano.2c01993
ACS Nano 2022, 16, 10566−10580

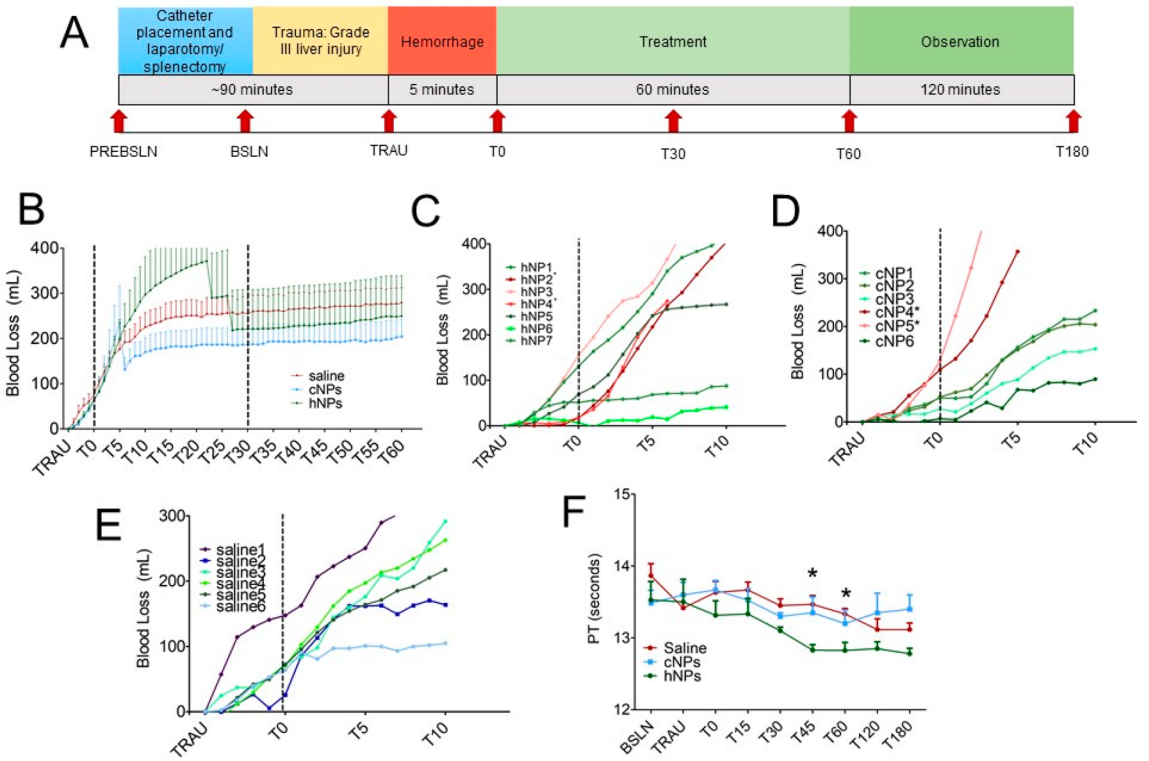

Figure 2. (A) Timeline for trauma model. The key parts include the hemorrhage followed by treatment or controls at T0, whole blood infusions between T30 and T60 to maintain blood pressure, and closure at T60 (error bars = SD, n = 6 per group). (B) Average cumulative blood loss across the groups, saline, control nanoparticles (cNPs), and hemostatic nanoparticles (hNPs). There are no significant differences in blood loss over the time period studied for any of the groups. (C) In our previous work, we found the first 10 min postadministration were critical for complement activation, which typically presents as greater blood loss because of the release of the vasodilators, C3a and C5a. Two animals in the hNP group show greater blood loss following the administration of the nanoparticles. (D) Likewise, two of the animals in the control group, cNP4 and cNP5, showed what looks like a small change in blood loss rate following nanoparticle administration, but the data are less clear, with a greater blood loss rate overall before the particle administration. (E) Blood loss for saline in the first 10 min. The saline2 animal shows an upturn in blood loss following saline administration. (F) Prothrombin time (PT) is lower for the hNPs than for controls, which suggests that the hNPs are hemostatic and reduce the time for blood to clot (*p < 0.05, error bars = SD).

controlled femoral artery bleed in a blood donor bag containing the anticoagulant citrate phosphate dextrose adenine solution (CPDA) at a 1:10 ratio for subsequent use in resuscitation. A standardized liver injury was created as previously described.[29] Briefly, to create this injury, the liver was isolated, and a ring clamp was placed on the lower aspect of the left lobe. A standardized liver laceration was created using the ring clamp as a guide, followed by removal of the lacerated lobe (approximately 25% of the liver lobe mass). The liver was allowed to spontaneously bleed in an uncontrolled manner for 5 min, with blood being removed via intraperitoneal suction and weight/volume quantified at 1 min intervals throughout hemorrhage and treatment phases. Figure 2A provides a timeline of all the events involved in the procedure.

At T = 0, the treatment or controls were administered. Nanoparticles were suspended in 30 mL of saline at 2 mg/kg and given as a bolus. At the 30 min time point, autologous whole blood (collected shed blood) was given as needed to maintain a systolic blood pressure (SBP) of 90 ± 5 mmHg. At T = 60 min, the liver injury was packed, and the abdomen was closed. Animals received maintenance fluids in the form of lactated Ringer's and were monitored under anesthesia until T = 180 min, when the animals were humanely euthanized.

Blood Loss and Physiological Parameters. There were no significant differences in blood loss for any of the groups (Figure 2B). Our previous work found that early blood loss data is important for assessing complement-mediated infusion reactions.[26] Complement activation leads to an increase in the rate of blood loss because of increases in the vasodilators C3a and C5a. There is a slight upturn in the hemostatic particle animals, hNP2 and hNP4, postparticle administration (Figure 2C). In contrast, in the control nanoparticle group, while cNP4 and cNP5 bleed more than the other control nanoparticle animals, there is no upturn in the blood loss postparticle administration (Figure 2D). Likewise, there are no upturns in the saline group (Figure 2E). Supplementary Figure 2 shows the individual animals' blood loss curves to help understand these responses. This upturn could be the result of the increase in the vasodilators C3a and C5a because of complement activation, but looking at blood loss, alone does not give a complete picture of complement activation.

A second important consideration regarding infusion reactions is changes in heart rate (HR) and mean arterial pressure (MAP) in concert with the change in blood loss rate.[26] The HR for the saline-treated animals was constant without spikes except in two animals following saline administration (Supplementary Figure 3A). Saline does not trigger complement, so the HR changes are because of other factors in these animals. In the control group, cNP4 and cNP5 show changes in HR, but several other animals show substantial changes as well without a change in blood loss

https://doi.org/10.1021/acsnano.2c01993
ACS Nano 2022, 16, 10566−10580

rate. In the hemostatic nanoparticle group, hNP2 and hNP4 show changes in HR as does hNP7, which survived to the end of the experiment and showed no change in blood loss rate upon particle administration. The MAPs for the saline-treated animals were very consistent throughout the experiment. The MAP for the cNP4 and cNP5 does not exhibit spikes but the animals died shortly after particle administration. However, there were small changes in the MAPs for the other cNP animals. Likewise, the MAP did not exhibit changes or spikes for hNP2 or hNP4 but did show small changes for other hNPs.

The HR and MAP results coupled with the increased bleeding in a subset of animals that received nanoparticles suggest that if complement activation is occurring, the impact is modest compared to those typically seen with complement activation following nanoparticle administration.[26] However, the nanoparticles were administered to animals undergoing a significant trauma, which could mask the effects of the nanoparticle administration. To rule out the impact of trauma, we looked at the impact of particle administration on a small set of naïve animals. Similar results to those seen in animals experiencing trauma were seen in the naïve animals with some changes in HR and MAP in the animals that received either control or hemostatic nanoparticles (Supplementary Figure 4.) To understand whether there were changes in complement or other molecules following nanoparticle administration, we performed ELISAs on serum isolated at 15 min intervals throughout the study.

Platelet Activating Factor (PAF) and Complement. Platelet activating factor (PAF) has been seen to trigger adverse physiologic effects following nanoparticle infusion including vasodilation and increased vascular permeability.[30] To investigate the role of PAF, we performed ELISAs on serum from the blood draws that were performed at 15 min intervals. None of the serum samples across animals or time points had detectable PAF. The limits of the PAF ELISA assay are 0.156 ng/mL.

While the HR and MAP data suggest that complement is either not activated or is activated at very modest levels, we performed ELISAs on the serum samples from the 15 min intervals for the animals that exhibited increases in blood loss following particle administration. Supplementary Figure 5 shows the complement results. If complement is activated, C3 should decrease and C3a should increase. In Supplementary Figure 5A, we see that the saline animal, for which there is no complement activation by blood loss or physiological data (Supplementary Figure 5C) shows some variation in C3 over time, but the changes are small compared to the 2−4-fold changes expected for complement activation. The changes seen in the saline animal are the same or greater than those seen for C3 in any of the animals that received nanoparticles. Likewise, the changes seen in C3a which should increase if complement is activated, are greater for the saline animal than any of the nanoparticle-animals (Supplementary Figure 5B). These data, taken with the physiological data suggest that complement activation is not occurring with the bolus administration of nanoparticles in this model.

Coagulation. Blood was collected at 15 min intervals from the start of the study through the first 60 min, and complete blood counts as well as coagulation tests were performed via the STAGO coagulation analyzer, ROTEM. The platelet counts were statistically identical for all the groups throughout the study (Supplementary Figure 6.) The hNPs led to a significant reduction in prothrombin time (PT) compared to either the saline or cNP groups at T = 45 and 60 min (Figure 2F). This finding indicates that globally, the hemostatic nanoparticles effectively reduce the time to clot formation beyond normal, adaptive physiologic hemostatic intrinsic to the animal. The half-life of the nanoparticles is relatively short, on the order of minutes.[31] Thus, it is not surprising that the impact of the nanoparticles is not seen at time points past T60. It is not surprising that the reduction is not fully resolved until the T = 45 min time point. There is a trend toward reduction before this, but the trend is not significant.

We found a similar trend toward a reduced PT in uninjured naïve animals (Supplementary Figure 7), although it must again be noted that the groups were very small (n = 3). While the hemostatic impact is not evident in the blood loss data in Figure 2B, it could be a function of the dose with a higher dose showing a more significant impact coupled with the fact that some of the animals that received particles had complications (Figure 3).

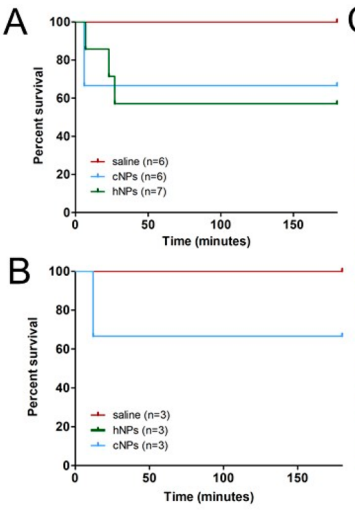

C

Animal number	treatment code	Clots
20-020M	saline	no
20-021M	saline	no
20-018M	saline	no
20-026M	saline	no
S20-032M	saline	no
S20-034M	saline	no
20-029M	cNP1	no
20-023M	cNP2	no
20-027M	cNP3	yes
S20-039*	cNP4	no
S20-038*	cNP5	yes
S20-046	cNP6	no
20-031M	hNP1	no
20-030M*	hNP2	no
20-022M*	hNP3	no
S20-042M*	hNP4	yes
S20-047M	hNP5	no
S20-037M	hNP6	yes
S20-040M	hNP7	yes

Figure 3. (A) Survival curves for treatments in the injured arm of the study (n = 6 per group). (B) Survival curves for the naïve arm of the study (n = 3 per group). (C) Table of animals, treatments, and clots as characterized by gross pathology and histology. Clots occurred in the brain, lungs, and kidneys of a subset of the animals receiving particle formulations. Animals noted with asterisks (*) died.

There are no differences in the partial thromboplastin time (PTT) or fibrinogen for any of the treatments in either the injured (Supplementary Figure 8) or naïve animals (Supplementary Figure 9). Likewise, no differences in d-dimer for any of the groups in the injured or naïve animals was seen. PTT measures clotting time based on the intrinsic pathway in contrast to PT, which is clotting time based on the extrinsic pathway triggered by tissue factor. Because the particles are designed to reduce bleeding by forming bridges akin to fibrinogen, they should not impact PTT, and so it reassuring to see that there are no changes in PTT with particle administration.[32] ROTEM results follow similar patterns to the STAGO coagulation results for PTT with no significant differences between groups or over time (Supplementary Figure 10).

While the reduction in PT with no changes in other coagulation parameters are promising data, administration of nanoparticles in this study was associated with reduced survival

https://doi.org/10.1021/acsnano.2c01993
ACS Nano 2022, 16, 10566−10580

in both the injured (Figure 3A) and naïve arms of the study (Figure 3B). Furthermore, pathology revealed that several of the animals that received particles exhibited clots in uninjured tissues including the lungs, kidneys, and brain (Figure 3C), perhaps indicating an abnormal systemic thrombotic or embolic phenomenon.

Survival and Clot Formation. All the animals in the saline group survived, but a subset in the control nanoparticle and hemostatic nanoparticle groups died within the first 30 min following particle administration. The first observation is that the animals died of hemorrhage. Animals that died bled more (13 ± 3.6 mL/kg) and those that lived (8 ± 2.6 mL/kg). At $T = 0$ when particles were administered, the group that survived exhibited similar blood loss on average to the group that died, but the cumulative blood loss varied significantly. The group that survived bled 1.4 ± 1 mL/kg and the group that died bled 1.9 ± 1.4 mL/kg. In only two animals, hNP2 and hNP4, was blood loss at $T = 0$ low (0.3 and 0.4 mL/kg, respectively.) In all the other animals that died, early cumulative blood loss was between 2.3 and 3.4 mL/kg. Excessive blood loss is lethal. However, there are animals that survived with blood loss equal to or greater than animals that died, indicating that hemorrhage alone may not have been the cause of the mortality. For example, animal hNP4 bled 9.3 mL/kg at death, but there are animals that bled more and yet survived (two saline animals and hNP6, Supplementary Table 3.) Typically, if blood loss is the cause of death, there will be a tipping point, a volume as a function of body weight, past which all animals would be expected to die. The fact that some animals bled less than others and died suggests that cumulative blood loss alone is not the entire answer for these early deaths.

If blood loss is not the entire answer, pathology becomes especially critical. In the gross pathology report, there were animals that had clots in a range of tissues (brain, kidneys, and lungs) that were hard nodules (Supplementary Figure 11). Histology confirmed that these hard nodules were not typical post-mortem clotting but were thrombi that occurred during the study. While these clots were seen in multiple tissues, every animal with the hard nodules had these thrombi in the caudal lungs, which is fed by the blood flow return from the heart. In contrast, no such thrombi were seen in the saline animals as described by the pathology reports based on gross pathology and the histological grading done by a pathologist blinded to the treatments. Representative hematoxylin and eosin (H&E) images of a saline animal cranial lung (Supplementary Figure 11C) and of lungs with thrombi (Supplementary Figure 11C–F) show examples of what appear to be thrombi at 40× magnification as marked by arrows. These H&E images also show extensive congestion in the lungs of these animals.

These thrombi were seen in both the control nanoparticle and hemostatic nanoparticle groups but not seen in the saline group. In both the control nanoparticle and hemostatic nanoparticle groups, these clots were seen in a similar number of animals and tissues. The clots do not appear to correlate with the presence of the GRGDS peptide on the nanoparticles that differentiates the hemostatic nanoparticles from the control nanoparticles (Figure 3C). The pathology suggests that these thrombi are a significant adverse event that may have contributed to the lethality seen in the nanoparticle groups. It should be noted that the pathological and histological grading was done by a pathologist blinded to the treatments and based on typical protocols for grading pathology and histological sections. Thrombi were not found in saline animals.

Looking at higher resolution specifically for thrombi led to the identification of microthrombi in the lungs of two animals with either control or hemostatic nanoparticles (Supplementary Figure 11G,H) that had not been identified previously based on gross pathology and grading of the H&E sections at lower magnification. Finding microthrombi is not entirely surprising. The secondary review was specifically looking for examples of thrombi in the lungs at higher magnification than previously used for the histological grading. These two animals were not included in the clot group for the correlation analysis because they did not present with pathological or histological findings consistent with thrombi during the initial review, but we note them to emphasize that the definition of thrombi used in the correlation analyses and subsequent analyses, while based on standard histopathological analyses, may not include every microthrombus present in the tissue.

Similar thrombi were seen in the naïve arm of the study in both the control and hemostatic nanoparticle groups suggesting that the trauma is not essential to trigger the formation of these hard nodule clots (Supplementary Table 4). Understanding what correlates with these thrombi is important to understanding how the nanoparticles impact outcomes.

One of the questions one might ask is whether the variation in size of the nanoparticles as measured by DLS (Supplementary Table 1) contributed to these outcomes. Supplementary Table 5 shows the average and standard deviation for all the nanoparticles as well as for those associated with clots and those associated with death. An ANOVA for both the cNPs and hNPs suggests there are no differences in size of nanoparticles involved in clots or survival.

Biodistribution across both injured and naïve animals showed similar patterns with no significant differences between animals with clots and animals without clots (Supplementary Figure 12.)

Data Science to Determine Parameters that Correlate with Lethality and Clot Formation. The critical question that arises from this, then, is what correlates with the clots? To investigate this, we performed a series of analyses using data science methods. Specifically, we used feature selection and random forest algorithms to identify features that are most predictive about the clots and survivability. While feature selection and random forests help us show the relationship to survivability and clots, the canonical correlation depicts the cluster if features which are correlated and the variables that are unique from the overlapping features.

Multiple forms of correlation analysis were used with the Luminex data, cell counts, clotting results, blood loss, and survival to determine what features correlated most often with the formation of clots and with survival. There was strong overlap of the factors influencing clots and survival even though there is partial overlap with animals. TNF-α, INF-α, IL-8, neutrophils, and lymphocyte changes correlated with survival and IL-6 correlated with clotting using a canonical correlation (Supplementary Figure 13C,D). We also performed feature selection using the machine learning algorithm, Random Forest. This is an ensemble algorithm that is composed of multiple decision trees. Decision trees create splits that maximize the reduction in impurity of a node for classification of an outcome feature (clot or survival). By calculating the mean decrease in impurity for each feature across all trees, we can know that feature's importance from our given data set. Feature importance techniques assign a score to independent features according to the role each

https://doi.org/10.1021/acsnano.2c01993
ACS Nano 2022, 16, 10566–10580

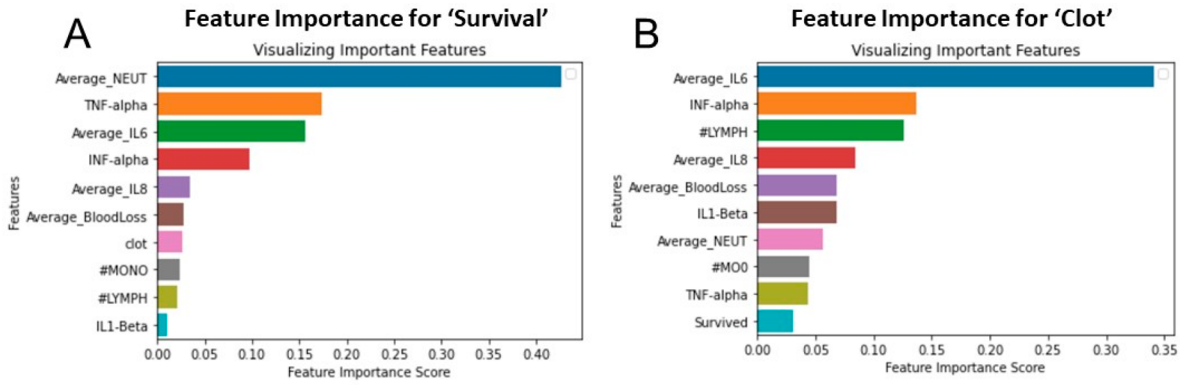

Figure 4. Multiple data science methods were used to look for correlations between survival and parameters measured in the study (cytokines, cells, and blood loss) and clot formation. A set of features rose to the top for all the feature selection methods that correlated with both survival and clot formation. These included IL-6, TNF-α, neutrophils, lymphocytes, IL-8, and INF-α. (A) Features of importance for survival. (B) Features of importance for clot formation.

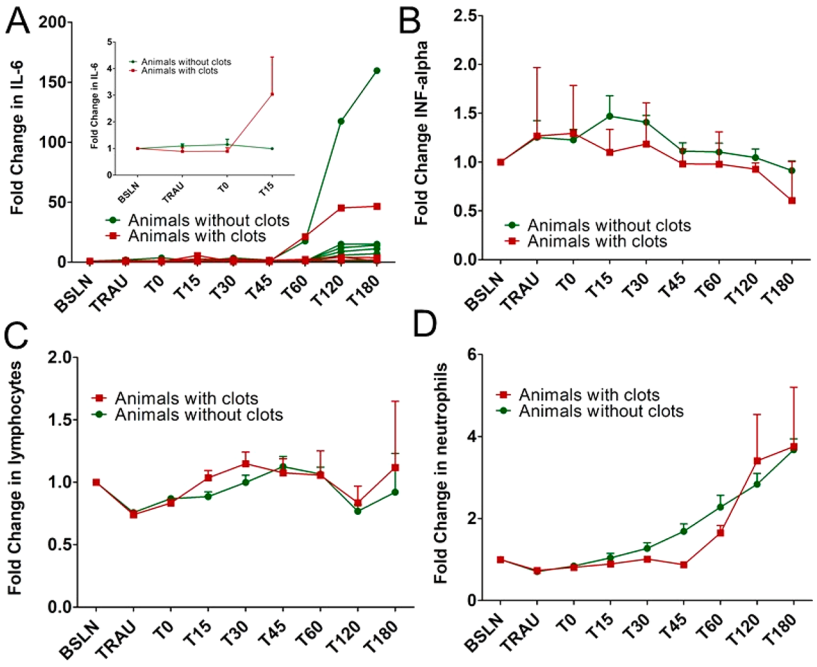

Figure 5. (A) Fold change in IL-6 over time as a function of whether clots were found post-mortem. Curves for individual animals are plotted to show the variation in responses along with the trends. Fifteen minutes post-treatment, animals who exhibited clots also showed an elevation in their IL-6 levels. (B) Fold change in the inflammatory cytokine, INF-α. Fifteen minutes post-treatment, animals that exhibited clots showed a small decrease in INF-α, whereas animals without clots showed an elevation in the INF-α level. (C) Lymphocytes increased more 15 min post-treatment for animals with clots than for those without. (D) Neutrophiles increased more for animals without clots than for those with clots. It should be noted that no blood draws were made post-mortem. (n = 6 and error bars = SD for panels A–D).

feature plays in predicting the dependent feature/target feature. Using this method, we found that Average_IL6 is listed as the top feature when we consider "clot" as the target feature whereas for the experiment where "survival" is the target feature we noticed that Average_Neut (neutrophils) is listed as the top feature (Figure 4A,B). Thus, across both canonical correlation and random forests, we saw a high correlation for IL-6 with clotting (Figure 4B and Supplementary Figure 13D) and a similar feature correlation for survivability (Figure 4C and Supplementary Figure 13C). Importantly, we saw similar trends in the naïve groups for important features (Supplementary Figure 13B), suggesting that these features are important for thrombi even in the absence of trauma, which further suggests that the nanoparticles are the critical factor. It should be noted that since these are large animal studies, the animal numbers are small for both the trauma and naïve arms of the study. Nonetheless, there is substantial heterogeneity in the data. This, coupled with multiple correlation analyses, lends credence to the importance of the features that repeatedly showed high correlation with the clot and survival outcomes.

In all correlation analyses, IL-6 was one of the most common features with a strong robustness regarding correlation. IL-6 increased in all groups over time with the fold change in IL-6 increasing the most for the hemostatic nanoparticle group (Supplementary Figure 14). A similar increase was seen in the naïve arm of the experiments primarily

https://doi.org/10.1021/acsnano.2c01993
ACS Nano 2022, 16, 10566–10580

driven by one animal that showed a substantial spike toward T = 120 min (Supplementary Figure 15).

Likewise, animals exhibited a significant increase in IL-6 values toward the end of the experiment in the injured arm whether they had clots or not with animals who did not show clots showing, on average, higher values (Figure 5A). At the earliest time points, animals with clots did show an increase at T = 15 min (inset of Figure 5A).

Both TNF-α and IL-8 showed up in many of the correlations for clot formation, but their values showed no clear trends with regards to the fold change in values. The data sets used are small and can be driven by outlier values, which seems to be the case with IL-8 that exhibited a few very high values (Supplementary Figure 16). TNF-α moved around a great deal, making patterns and trends unclear (Supplementary Figure 17).

In looking through the top correlates with clot formation or survival, the four parameters that stood out were IL-6, INF-α, lymphocytes, and neutrophils. The early trends in IL-6 suggest that an increase correlates with clot formation (Figure 5A). That is not surprising because an increase in IL-6 has been correlated with clot formation in deep vein thrombosis[33−35] as well as COVID-19.[36] One of the questions that is raised is whether there are early changes in IL-6 that may correlate with an infusion response. IL-6 does increase in this study for animals that exhibited clots over the first 15 min, but this observation is based on a very small data set. The data sets are extremely small because the clots are only seen in a subset of the animals that received nanoparticles but in both the control and hemostatic groups in similar numbers (n = 2 for the control group and n = 3 for the hemostatic group). However, it would be wise to look at early IL-6 changes in future studies because the increase may be important for understanding potentially adverse outcomes that may be related to nanoparticle infusions.

Focusing on the first 30 min post-particle administration when infusion responses are often seen, we observe that INF-α increases following treatment in animals without clots but stays constant or decreases slightly for animals with clots. Increases in INF-α has been correlated with thrombi in several models of disease,[37−39] which makes the fact that the increase correlates with animals that did not exhibit clots surprising although at the longer time points INF-α decreased in all the animals studied (Figure 5B). Lymphocytes increased more 15 min post-treatment for animals with clots than for those without (Figure 5C). In contrast, over early time points, the number of neutrophils were lower for animals with clots than those without (Figure 5D). The changes in these values were not seen from the naïve arm of the study, but the naïve groups were extremely small (n = 3 per group for n = 9 total with two animals exhibiting clots, Supplementary Figure 15). This follows the trend that there were no changes seen in naïve animals, with respect to IL-6 in the first 15 min (Supplementary Figure 15.) Of course, the caveat with all of this is that the animal numbers are small. While the heterogeneity, multiple methods, and repeated correlations suggest that these factors have high correlation with the clot and survival findings, it is important to be cautious about drawing conclusions from the specific changes in this small data set. Instead, we present this data not to over interpret the findings but to provide a basis for understanding the underlying data that correlates with the outcomes regarding clots and survival following nanoparticle infusions in this work.

As noted, the same factors that correlate with survival correlate with clot formation even though there is only partial overlap between the animals that die and those with clots. Said another way, the group that died included both animals with clots and animals without clots. Nonetheless, looking at survival/death, IL-6 decreased slightly for animals that died, but the blood draw was immediately before death and other processes may confound the results. Neutrophils were also lower for animals that died immediately before death (Supplementary Figure 19), thus following the same trend seen with clot formation.

Parameters that Correlate and In Vitro Screening. The PEGylated polyester nanoparticles used in this study correlated with negative outcomes independent of whether they had the GRGDS peptide or not (both the hemostatic nanoparticles and control nanoparticles). Not all animals that received polyester nanoparticles had negative outcomes (death and/or clots) but a subset did. In contrast, the vehicle control group did not exhibit similar negative outcomes. While we did not see complement activation in vivo, there were signs of inflammatory processes that correlated with the firm clots and negative outcomes.

By looking at the data via correlation analysis and coupling that with an analysis of the findings, it appears that changes in IL-6, INF-α, lymphocytes, and neutrophils correlate with negative outcomes in vivo with nanoparticles. To gain more insight into the role polyester nanoparticles may be playing in vivo, nanoparticles or controls were incubated with heparinized whole blood and a cytokine array assay was performed.

The cytokines represented are those that showed positive spots in the array (Figure 6). This method is pseudoquantitative and leads to intensities rather than absolute values of

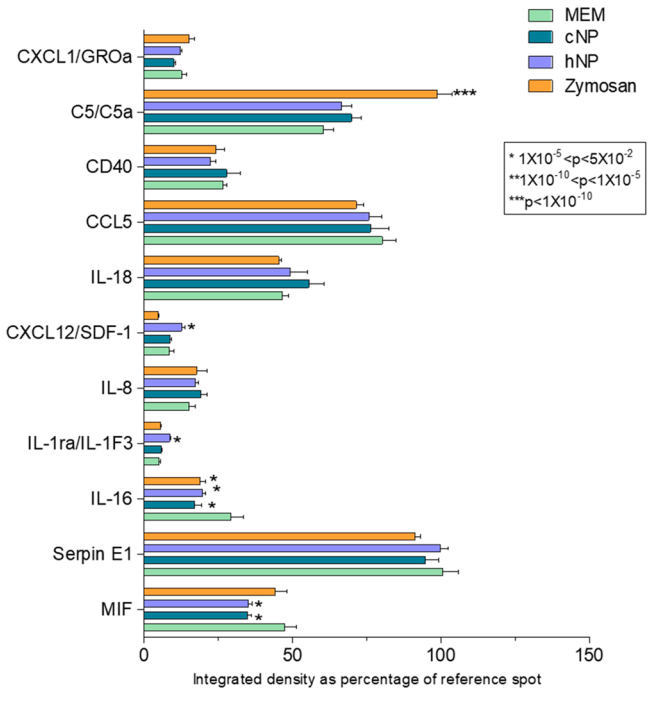

Figure 6. Cytokine profiler array. Change in cytokines for heparinized human whole blood incubated with control and hemostatic nanoparticles. Change in complement protein C5/C5a was most significant for zymosan based on χ^2 analysis (error bars = SD).

https://doi.org/10.1021/acsnano.2c01993
ACS Nano 2022, 16, 10566−10580

cytokines. No spots were seen for IL-6 or for TNF-α, and the kit does not include INF-α. Nonetheless, there are points of connection to the in vivo findings that are important to explore. C5/C5a is positive for zymosan, which is expected because zymosan is a positive control for complement. The levels for the control and hemostatic nanocapsules are the same as the negative control, minimum essential medium (MEM). The hemostatic nanoparticles but not the control nanoparticles, MEM, or zymosan are positive for CXCL12/SDF-1. SDF-1 is known to upregulate TNF-α.[40] Likewise, the hemostatic nanoparticles but not the control nanoparticles, MEM or zymosan are positive for IL-1ra/IL-1F3. The Interleukin-1 receptor antagonist (IL-1ra) can reduce acute inflammation following trauma[41] and dampen inflammation in diseases such as rheumatoid arthritis.[42] Neutrophils are known to release IL-1ra, IL-16, and MIF when undergoing cell death.[43] IL-16 is lower for zymosan, and both the hemostatic and control nanoparticles compared to MEM. Interleukin-16 (IL-16) is a chemoattractant factor[44] released in response to mitogens, antigens, or vasoactive amines such as histamine or serotonin.[44] IL-16 induces upregulation of pro-inflammatory cytokines (IL-1β, IL-6, and TNF-α).[45] Downregulation of IL-16, as is seen here, is associated with a reduction in lymphocyte migration.[46] Macrophage migration inhibitory factor (MIF) activates neutrophils.[47] The downregulation of MIF in the nanoparticle groups is significant and may lead to modulation of the immune response that, especially in the presence of trauma, leads to a reduction in neutrophils, which we saw correlated with worse outcomes following particle administration (Figure 5D).

We designed the study to focus on blood loss with complete survival of the saline group. As blood loss becomes more severe and patients progress toward death, there are several factors that occur including trauma induced coagulopathy and the lethal triad.[48−50] While these are extremely important to model and understand, they significantly increase the complexity of the model and assessments. Therefore, we chose a more conservative bleeding model as a first step in assessing the safety and efficacy of these nanocapsules.

We tested the hemostatic nanoparticles, control nanoparticles, or saline in a porcine liver injury model, and examined the impact of these nanoparticles on blood loss, physiological outcomes, coagulation parameters, immune cell responses, and cytokine arrays. We also included a naïve arm of the study in which we administered our hemostatic nanoparticles, control nanoparticles, or saline in the absence of a trauma to determine whether off-target effects were the result of a combination of the particles and trauma or a result of the particles alone. While we found that the hemostatic nanoparticles did positively impact coagulation parameters, there were off-target effects leading to nonspecific clotting. We applied a series of approaches from data science to understand the correlates with these clotting events as well as survival to determine the off-target mechanism triggered by these polyester nanoparticles.

The ultimate goal of our work is to lay the groundwork for treatments for severe bleeding in the context of trauma. Stopping bleeding in rodents with nanotechnologies has been achieved with several different approaches[7,21,31,51−54] even in the context of thrombocytopenic conditions.[54] But, stopping bleeding in clinically translatable large animal models in a safe manner has proven very challenging. We have known for some time that complement activation was a hurdle.[20,26,55,56] In this work, we looked at nanoparticles that do not activate complement.[28] While these particles did not activate complement in vitro or in vivo, their administration unmasked other challenges that must be addressed.

The animal numbers in this study are small, which can lead to challenges in having the data to power results, but it is clear that early changes in IL-6, INF-α, lymphocytes, and neutrophils are potentially significant and should be considered carefully in designing and testing nanomaterials to treat trauma and nanomaterials for intravenous administration more broadly. We know that IL-6 correlates with worse outcomes in trauma,[57] but what we are seeing with regards to thrombi is not limited to trauma. The hard nodule clots were seen in the naïve groups that received particles as well, and data science to look for correlations found similar patterns with the naïve arm of the study as were seen in the injured arm of the study. Thus, the findings that polyester-based, PEGylated nanoparticles can cause serious, adverse events goes beyond the complex milieux of trauma.

How can we begin to develop screening systems to look at the safety of nanoparticles for translation based on these findings? We have previously seen that incubation of polyester nanoparticles with endothelial cells leads to a decrease in IL-6[28] similar to what is seen in the naïve arm of the study. In vitro screens like this play an important role in understanding how nanoparticles impact outcomes. There are already elegant assays to look at the interactions between neutrophils and microparticles[58−61] as well as lymphocytes and micro/nanoparticles[62−64] that can be leveraged to understand the mechanisms involved in these interactions and screen for safety for nanotechnologies.

One of the surprising findings in the work was that we saw a reduction in neutrophils in animals that exhibited thrombi. Neutrophils are associated with increases in coagulation factors including PTT and can promote clotting.[65] However, we saw no changes in PTT and, in fact, fewer neutrophils in early times post-particle administration correlated with thrombi in this model. In contrast, we saw an increase in lymphocytes. Thus, the neutrophil to lymphocyte ratio (NLR) was decreasing at early time points following administration of particles. Again, this contrasts with the elevated NLR that has been seen associated with clot formation both in COVID-19 and in patients with admission to the ER with cardiopulmonary distress.[66−68] On the basis of the wealth of literature and small changes in the findings, while neutrophils and lymphocytes are clearly important in the thrombi, the changes in these cells following nanoparticle administration are small, and confidence in suggesting how they change and how that impacts outcomes is small. Studies looking at neutrophil and lymphocyte interactions with nanoparticles will be an important part of understanding these interactions.

This is a pilot study, and it is possible that the limited number of animals could lead to results that are not fully replicated at scale, but the key point is that the changes in cytokines, lymphocytes, and neutrophils are important to screen for in vitro moving forward with nanomaterials to ensure safety.

One of the caveats that must always be considered when dealing with porcine models is that their innate immune and thrombotic responses are often more intense than humans' responses. Infusion reactions tend to be more intense in porcine models than those seen in the clinic.[69,70] Such responses are often magnified by the speed of the infusion,

https://doi.org/10.1021/acsnano.2c01993
ACS Nano 2022, 16, 10566−10580

which in this study was a bolus. Bolus infusions are preferred when one is managing trauma, but they may magnify the impact of nanomaterials given systemically. Furthermore, swine appear to have earlier and more intense activation of pro-thrombotic mechanisms compared to humans and have limited thrombolysis capacity.[71,72] Nonetheless, the findings here point to potential adverse events that must be studied and considered when developing intravenously infusible nanomedicines.

Ultimately, if the goal is to control bleeding in models of trauma, the challenge goes beyond stopping bleeding. Acutely bleeding trauma patients are well-known to also be hypercoagulable from systemic activation of pro-coagulant mechanisms. Furthermore, trauma patients can rapidly switch between hypocoagulable and hypercoagulable depending on intrinsic physiologic factors, external factors such as the rate and extent of blood loss, and environmental factors such hypothermia.[5,50] Thus, pharmacologic or technology solutions that only stop bleeding could increase complications or even worsen outcomes. These conditions include disseminated intravascular coagulation (DIC),[73] trauma-induced coagulopathy (TIC),[74,75] and traumatic brain injury (TBI).[76−78]

Triggered by trauma as well as sepsis, DIC leads to inflammatory reactions, endothelial dysfunction, and generalized thrombosis causing organ damage and failure and poor patient outcomes.[73] With DIC, a patient can transition rapidly from a hypocoagulable to hypercoagulable state. In trauma patients, the complex interplay of tissue injury and hemorrhagic shock combine to create TIC,[79] also known as acute traumatic coagulopathy. TIC occurs rapidly in 20−35% of severely injured trauma patients[80] when protein C is activated and inhibits the clotting cascade through cleaving factors Va and VIIIa. Factor Va is part of the prothrombinase complex that cleaves prothrombin into thrombin, a critical component for hemostasis. Activated protein C also accelerates fibrinolysis and leads to platelet dysfunction.[81,82] Rapid surgical intervention is essential to stop the contribution of ongoing blood loss to the cycle of TIC.[83,84]

The complexity of these challenges is further exacerbated by TIC-associated hypercoagulability, potentially a result of endothelial damage leading to a reduction in tissue-type plasminogen activator (tPA).[85−87] Finally, the extent of hemorrhaging in TBI has been correlated with the degree of functional deficits following central nervous system trauma in humans[88,89] and with the extent of injury in rodent models.[88,90] Again, the challenge with halting bleeding is that TBI patients can rapidly switch back and forth between hypocoagulable and hypercoagulable states,[76−78,91] and while research is ongoing, predicting the transitions is extremely difficult.[92,93] In addition, TBI brain microparticles can induce systemic coagulation including pulmonary emboli.[94]

CONCLUSIONS

Thus, as we look to develop therapies to manage bleeding, we have a high bar to meet. The therapies must be safe and avoid adverse events in an extremely complex environment. The need is there to tackle this challenge, though, with trauma and uncontrolled bleeding being the leading cause of death of young people. This work elucidates some of the cellular and molecular responses that should be considered in developing nanotechnologies to control bleeding.

The complexity of administering nanomedicines intravenously may be changing as well. The potential impact of COVID-19 on endothelial dysfunction, clotting disorders, and thrombi.[95−97] As we translate infusible nanotechnologies in patients who have had COVID-19, we may find that the safety profile for these patients has changed. Being able to screen nanotechnologies at early stages for cytokine and immune cell responses has the potential to lay a framework for safer nanomedicines more broadly, beyond the complex milieux of trauma.

EXPERIMENTAL SECTION

Materials. A poly(lactic acid)-*b*-poly(ethylene glycol) block copolymer was synthesized using L-lactide from Polysciences Inc. (Warrington, PA), heterobifunctional poly(ethylene glycol) with 5000 and 3400 Da molecular weight from Laysan Biosciences (Arab, AL), and D-lactide from Purac Biomaterials (Corbion, Amsterdam, Netherlands). All solvents used were of ACS grade and obtained from Fisher Scientific.

We monitored Complement protein C5a using a C5a human ELISA duo kit (DY2037) obtained from R&D Systems (Minneapolis, MN). Zymosan was obtained from Sigma-Aldrich. Dulbecco's phosphate-buffered saline (without phosphate and magnesium) was obtained from Fisher Scientific. We measured cytokine levels in vitro using Proteome Profiler Human Cytokine Array Kit (R and D Systems, catalog number ARY005B). For in vitro assays, as blood matrix, we used heparinized human blood and complement protected human serum from Innovative Research Inc. (Novi, MI).

Synthesis and Characterization of Nanoparticles. Block copolymers of poly(lactic acid)-*b*-poly(ethylene glycol) with either 3400 or 5000 Da PEG macroinitiators was synthesized through the ring-opening polymerization reaction.[21,98] The nanoparticles were prepared using poly(L-lactic acid)-*b*-poly(ethylene glycol) (PLLA-*b*-PEG5000) and poly(D-lactic acid)-*b*-poly(ethylene glycol) (PDLA-*b*-PEG3400) through nanoprecipitation. The numbers denote the molecular weight of the PEG macroinitiator, i.e. 3400 and 5000 Da. The peptide GRGDS was conjugated through NHS/EDC conjugation to PLLA-*b*-PEG5000.[21]

The ratio for the polymers is 3:1 by weight. Here 90 mg of PLLA-*b*-PEG5000 and 30 mg of PDLA-*b*-PEG3400 was used for making the control and hemostatic nanoparticles. The polymer was dissolved in the organic phase, i.e. tetrahydrofuran (THF), at a concentration of 20 mg/mL was added dropwise to double the phosphate-buffered saline's volumetric amount and stir hardened to form the nanoparticles. After stir-hardening for 3 h, excess THF was removed by exposing to air, and poloxamer was added as the stabilizer. The nanoparticles were then collected through centrifugation at 4000XG for 10 min at 4 °C and resuspended in phosphate-buffered saline. The particles were characterized through dynamic light scattering for determining the hydrodynamic diameter and the ζ-potential for nanoparticles in dilute potassium chloride solution (10 mM). The extent of PEGylation was determined through ^{1}H nuclear magnetic resonance as well. The control nanoparticles were prepared in a similar manner, but instead of peptide conjugated PLLA-*b*-PEG5000-GRGDS, the block copolymer PLLA-*b*-PEG5000 was used.

Conjugation of GRGDS to PLLA-*b*-PEG through NHS/EDC Coupling. The peptide of interest, GRGDS, was conjugated to the block copolymer PLLA-*b*-PEG5000 through NHS/EDC conjugation. Utilizing the carboxyl end of the bifunctional PEG, the NHS/EDC based conjugation leads to coupling with the amine end of the peptide GRGDS. First, 300 g of the block copolymer PLA-*b*-PEG is dissolved in 4 mL of dichloromethane (DCM). To that was added 12 mg of NHS and 10 mg of EDC dissolved in dimethyl sulfoxide (DMSO) to form an amine-reactive NHS-ester. The reaction was allowed to proceed for 60 min, and then excess DCM is removed by exposure to air. The polymer was precipitated in methanol and collected by centrifugation at 4000 rpm for 5 min and lyophilized overnight. The lyophilized intermediate product was dissolved in 3 mL of DCM and to that was added 8 mg of the peptide dissolved in 1.5 mL of DMSO. The reaction was allowed to proceed for 24 h, and then the excess DCM was removed by exposure to air, and the polymer was

https://doi.org/10.1021/acsnano.2c01993
ACS Nano 2022, 16, 10566−10580

precipitated in methanol. The precipitated PLLA-*b*-PEG-GRGS was the collected through centrifugation at 4000 rpm for 5 min and lyophilized.

Measuring Peptide Density Using OPA Assay. The presence of peptide in the nanoparticles was confirmed through an orthopthaladehyde (OPA) assay, which leads to fluorescence in the presence of free amines. Here 200 μL of OPA reagent was added to 20 μL of nanoparticles dissolved in DMSO and mixed well. The fluorescence was recorded immediately after 15 min of incubation in the dark using an excitation wavelength of 340 nm and emission wavelength of 455 nm.

Handling of Blood Products. For generating the responses in vitro, the heparinized human whole blood and complement protected human serum used was obtained from Innovative Research Inc. (Novi, MI). In the case of whole blood, blood was collected in heparinized collection tubes from a single donor and shipped using the same collection vial to avoid exposure to multiple surfaces and lead to unwanted complement activation. Blood was handled with care, stored, and shipped at 4 °C, and only mixed gently, and stored on ice while running the assay.

Evaluation of Changes in Complement Protein In Vitro. The change in complement protein C5a was quantified following previously established protocol.[27] The blood matrix was incubated with nanoparticles suspended in Dulbecco's PBS (without calcium and magnesium). As a positive control, zymosan was used. The dosage used for the nanoparticles and zymosan was 0.25 mg/mL in serum. The samples were incubated at 37 for 45 min and then centrifuged at 4000 rpm for 5 min to separate the nanoparticles. The plasma was aliquoted in clean tubes and stored on ice until assay was carried out.

Ethical Approval and Accreditation. The study protocol was reviewed and approved by the 711th HPW/RHD JBSA-Fort Sam Houston Institutional Animal Care and Use Committee (IACUC) in compliance with all applicable Federal regulations governing the protection of animals in research. All procedures were performed in facilities accredited by the AAALAC international.

Power Analysis. We designed the experiment to looks for differences in hemorrhage rather than survival. Because this was a large animal porcine study, we used a resource equation method to power the study. This approach is considered appropriate when designing resource-intensive large animal studies and/or those that involve potential ethical concerns. In this approach, Error = Total number of animals − Total number of groups with the ideal target for Error (E) being between 10 and 20. In our experimental design, E = 18−3 = 15 with n = 6 per group. Conversely, using a conventional power analysis, assuming that reducing blood loss by 0.3 L in pigs would be significant based on previous work where the standard deviation in blood loss was 0.2 L, we would find that we need 7 pigs per group. Thus, the calculations are close, but considering the negative outcomes, the complexity of trauma models in large animals, and the resources, we focused on the resource equation method for calculating sample size and ended the study with 6 animals per group.

Animal Subjects and Preoperative Preparation. Thirty male swine (Sus Scrofa domesticus) weighing 35−60 kg were randomized and blinded into two injury arms each containing three treatment groups: (1) Injured Arm 1.a, vehicle control (normal saline, 0.9% NaCl) (n = 6); 1.b, 2 mg/kg control nanoparticles (n = 6); 1.c, 2 mg/kg hemostatic nanoparticles (n = 7) or (2) Uninjured Arm 2.a, vehicle control (normal saline, 0.9% NaCl) (n = 3); 2.b, 2 mg/kg control nanoparticles (n = 3); 2.c, 2 mg/kg hemostatic nanoparticles (n = 3).

Animals were sedated with Telazol (6.0 mg/kg; Fort Dodge Animal Health, Overland Park, KS, USA), premedicated with an analgesic (Buprenex 0.01 mg/kg; Reckitt & Colman Pharmaceuticals Inc., Richmond, VA, USA), and intubated with anesthesia maintained on 1−3% isoflurane. Core body temperature was monitored via a rectal temperature probe and maintained between 36.0 and 38.0 °C.

Catheter Placement, Laparotomy and Splenectomy. Four catheters were placed percutaneously under ultrasound guidance. Briefly, two 8 Fr catheters (Arrow, Morrisville, NC, USA) were placed in the jugular veins for fluid infusion and treatment administration and central venous pressure monitoring (CVP). Femoral arteries were cannulated with either a 5 Fr catheter (Cook Medical, Bloomington, IN, USA) for blood pressure monitoring (MAP), or an 8 Fr catheter (Arrow, Morrisville, NC, USA) for blood collection and sampling.

A midline laparotomy was performed to expose the spleen and liver. The left upper quadrant of the spleen was identified and mobilized to the midline. The splenic vein and artery were clamped off. All surgical procedures were performed under aseptic techniques.

Whole Blood Collection. Before injury, 30% total blood was collected from a controlled femoral bleed in a blood donor bag containing anticoagulant citrate phosphate dextrose adenine solution (CPDA) at a 1:10 ratio for subsequent use in resuscitation.

Injury and Hemorrhage. For the Injured Arm, a standardized grade III liver injury was created as previously described by Gurney et al.[29,99] Briefly, the liver was isolated and a ring clamp placed over the lower left lobe, ∼50% in width and ∼2.0 in. from the apex, adjusting for relative size of the liver and weight of the pig. The clamp was closed, and an 11 blade was used to lacerate the lobe from the top of the clamp through the remaining width, marking the beginning of hemorrhage. After 1 min the clamp was removed and the rest of the tissue excised, resulting in ∼25% lobectomy. Excised tissue was measured and weighted. The liver was allowed to spontaneous bleed for 5 min, with blood being removed via intraperitoneal suction and weight/volume quantified at 1 min intervals through hemorrhage and treatment phases.

Treatment, Resuscitation, and Euthanasia. Treatment was initiated at T = 0 min via a 30 mL bolus of either (1) 0.9% NaCl, (2) 2 mg/kg control nanoparticles, or (3) 2 mg/kg hemostatic nanoparticles. Additional fluids were postponed for 30 min, at which point whole blood was given as needed to maintain a systolic blood pressure (SBP) of 90 ± 5 mmHg. The initial whole blood transfusion was preceded with a 23% calcium gluconate solution (Vedco, Saint Joseph, MO, USA) at 1 mL/200 mL based on the 30% whole blood bleed.

At the end of treatment (T = 60 min) liver injuries were packed, closed, and animals received maintenance fluids in the form of lactated Ringer's and were monitored under anesthesia until T = 180 min. Swine were humanely euthanized at T = 180 min with pentobarbital sodium and phenytoin sodium (Euthasol, 390 mg/mL, Virbac Corporation, Fort Worth, TX, USA).

Blood Draws and Laboratory Analysis. Whole blood was collected as BSLN, TRAU, T = 0, 15, 30, 45, 60, 120, and 180 min. No blood draws were made post-mortem. Arterial blood gas parameters were assessed utilizing a GEM Premier 4000 (Instrumentation Laboratory, Bedford, MA, USA). Complete blood counts, basic metabolic panels, and liver associated enzymes were evaluated on ProCyte Dx Hematology and Catalyst One Chemistry Analyzers (IDEXX Laboratories, Inc., Westbrook, ME, USA).

Whole blood viscoelastic clotting properties were evaluated by rotational thromboelastometry (ROTEM) (ROTEM Delta system, TEM Systems Inc., Durham, NC, USA). ROTEM analyses included evaluation of extrinsic coagulation pathway function in the absence (ExTEM), presence of the platelet inhibitor, cytochalasin D (FibTEM), and the presence of the fibrinolysis inhibitor, aprotinin (ApTEM) including clotting time (CT), amplitude 10 min after CT (A10), amplitude 20 min after CT (A20), clot formation time (CFT), maximum clot firmness (MCF), alpha-angle (α), lysis index 30 min after CT (LI30), lysis index 60 min after CT (LI60), and maximum lysis (ML).

Concentrations of coagulation factors were evaluated using STAGO STA Compact (Diagnostica Stago Inc., Parsippany, NJ, USA). STAGO analysis included prothrombin (PT) and partial thromboplastin (PTT) times, and concentration levels of d-dimer, fibrinogen, von Willabrand Factor (vWF), and antithrombin (ATIII).

EDTA plasma was separated from remaining whole blood samples and divided into aliquots for subsequent Luminex analysis, which included interferon (INF) INF-γ, INF-α, interleukin (IL) IL-1β, IL-10, IL-12p40, IL-4, IL-6, IL-8, and tumor necrosis factor alpha (TNF-α) (Invitrogen Cytokine and Chemokine 9-Plex Porcine ProcartaPlex Panel 1, ThermoFisher Scientific, Waltham, MA, USA). Cytokine and

https://doi.org/10.1021/acsnano.2c01993
ACS Nano 2022, 16, 10566−10580

chemokine concentrations were quantified using the Bio-Plex 200 Luminex system (Biorad, Hercules, CA, USA).

Nanoparticle Bioaccumulation and Biodistribution. During necropsy, 1 cm cubes of tissues were collected and flash frozen for subsequent nanoparticle biodistribution analysis, which included liver, kidney, cranial lung (left and right), caudal lung (left and right), frontal cortex, occipital cortex, cerebellum, hippocampus, mesenteric lymph nodes, and gastrohepatic lymph nodes. The 1 cm cubes of tissue were kept at −80 C until biodistribution was performed.

Preparing Tissue Samples. Each 1 cm cube (one per tissue from the center of the tissue) was rinsed with deionized water 3 times. Samples were placed into preweighed 50 mL tubes and placed at −80 °C for 2 h to freeze. Samples were then lyophilized. Following lyophilization, each sample was weighed to determine the dry weight. The samples were transferred into homogenizing tubes and homogenized (Precellys 24; 6500 rpm, 2 cycles, 20 s per cycle, 5 s wait time between cycles). Samples were resuspended in 1 mL of acetonitrile, and homogenization was repeated. Samples were then kept at 37 °C for 48 h. After incubation, the samples were centrifuged at 13.3 rpm for 10 min. The supernatant was transferred to eppendorf tubes. The samples were diluted 1:10 with ACN and read using the plate reader at an excitation of 387 nm and emission of 470 nm (Molecular Devices, Spectramax M2). A standard curve of C6 in ACN was used to determine the concentration of C6 and the amount per mg of tissue. Knowing the loading of C6 in the nanoparticles, the concentration of nanoparticles per mg of tissue was determined.

Tissue Preparation and Pathology. Immediately following euthanasia, full necropsies were performed by veterinarian pathologists for gross and microscopic anatomic evaluation on each animal. Lung tissues were collected for histopathologic evaluation. These tissues were fixed in 10% neutral buffered formalin; paraffin embedded, cross sections were cut at 5 μm, and stained with H&E. A pathologist blinded to the treatments reviewed and scored the pathology and histological sections.

Complement Assays and PAF Assay on Serum Samples from In Vivo Study. Serum samples were stored until use. Serum samples were aliquoted and only used once to avoid freeze−thaw cycles. Samples were taken from the storage condition of −80 °C immediately before the ELISA assay was carried out. They were placed in 37 °C for few seconds to thaw immediately. Four different dilutions were used: undiluted, 1:1, 1:50, 1:1000. The standards were also prepared following the kit instructions. PAF was quantified using the pig specific kit from LifeSpan BioSciences, Inc. (Seattle, WA, Catalog no. LS-F37444). C3 and C3a were quantified using Abcam kits we had used previously with pigs (Abcam ab157705 and ab133037, respectively).[26]

Generating Immune Response In Vitro and Quantification through Cytokine Array. Nanoparticles resuspended in MEM were added to human heparinized whole blood to reach a final concentration of 0.25 mg/mL. The ratio of blood to the nanoparticle in MEM was 5:1. The blood was gently pipetted with the nanoparticle resuspension and incubated for 45 min at 37 °C in a rotating shaker. Immediately after incubation, samples were placed on ice and then centrifuged at 4000 rpm for 5 min. The supernatant plasma was collected in clean microcentrifuge tubes. For the cytokine array panel, 200 μL of plasma was used to prepare samples following the protocol, and subsequent steps given in the protocol were followed for the human cytokine array panel (R&D Systems). The final image was taken using a Bio-Rad imager. For further analysis, ImageJ was used. Integrated density gives the sum of total pixels within a region. Following this method, each dot blot within the membrane was quantified for each sample The levels of the detected cytokines were expressed as a percentage of the pixel density determined for the reference spot.[100]

Data and Statistical Analysis. Statistical analyses were performed using Prism 8 (GraphPad Software, Inc., La Jolla, CA, USA). Data are presented as mean ± SD. Data with baseline discrepancies were normalized to baseline before statistical analysis. Single time point analyses were performed by one-way ANOVA using posthoc Tukey and multiple time point analyses were analyzed by mixed-effects analysis using posthoc Tukey for intra-analysis and Dunnet for interanalysis.

Data Science. We carried out canonical correlation analysis experiments both in R Studio and Python. Packages exist in R Studio and Python, which create a visualization showing highly correlated variables. Independent attributes that are highly correlated to the target attribute are present near the target attribute.

Multiview Learning. Multiview learning is a domain where we identify relations between related data sets. This technique aids in identifying important attributes toward the target attributes. Multiview learning includes various types of techniques. Few among these popular techniques are canonical correlation analysis and matrix factorization.

Canonical Correlation Analysis. We carried out the canonical correlation analysis experiment on the porcine data. Canonical correlation analysis gives us a better idea of correlations that exist between two data sets. Canonical correlation analysis consists of two core parts, namely identifying canonical variables and canonical correlation among variables.

ASSOCIATED CONTENT

Supporting Information

The Supporting Information is available free of charge at https://pubs.acs.org/doi/10.1021/acsnano.2c01993.

> Details regarding every batch of nanoparticles synthesized and used in this work, blood loss data, physiological data, coagulation results, cell counts and cytokines for both injured and naïve pigs, and histological findings; figures regarding correlation analysis findings are also included (PDF)

AUTHOR INFORMATION

Corresponding Author

Erin B. Lavik − *UMBC, Baltimore, Maryland 21250, United States;* orcid.org/0000-0002-0644-744X; Email: elavik@umbc.edu

Authors

Nuzhat Maisha − *UMBC, Baltimore, Maryland 21250, United States*

Chhaya Kulkarni − *UMBC, Baltimore, Maryland 21250, United States*

Narendra Pandala − *UMBC, Baltimore, Maryland 21250, United States*

Rose Zilberberg − *UMBC, Baltimore, Maryland 21250, United States*

Leasha Schaub − *Naval Medical Research Unit-San Antonio, San Antonio, Texas 78234, United States*

Leslie Neidert − *Naval Medical Research Unit-San Antonio, San Antonio, Texas 78234, United States*

Jacob Glaser − *Naval Medical Research Unit-San Antonio, San Antonio, Texas 78234, United States*

Jeremy Cannon − *Hospital of the University of Pennsylvania, Philadelphia, Pennsylvania 19104, United States*

Vandana Janeja − *UMBC, Baltimore, Maryland 21250, United States*

Complete contact information is available at: https://pubs.acs.org/10.1021/acsnano.2c01993

Notes

The authors declare no competing financial interest.

ACKNOWLEDGMENTS

We thank Nidhi Naik and Tobias Coombs for their help synthesizing and characterizing the particles for the study. This work was supported by the AIMM Research award (DOD) (Award Number# W81XWH1820061) and by NIH R56 Grant (Project# 1R56NS100732-01).

REFERENCES

(1) Krug, E. G.; Sharma, G. K.; Lozano, R. The global burden of injuries. *Am. J. Public Health* **2000**, *90* (4), 523−526.
(2) Sauaia, A.; Moore, F. A.; Moore, E. E.; Moser, K. S.; Brennan, R.; Read, R. A.; Pons, P. T. Epidemiology of trauma deaths: a reassessment. *Journal Of Trauma-injury Infection And Critical Care* **1995**, *38*, 185−193.
(3) Champion, H. R.; Bellamy, R. F.; Roberts, C. P.; Leppaniemi, A. A profile of combat injury. *J. Trauma* **2003**, *54* (5 Suppl), S13−S19.
(4) Regel, G.; Stalp, M.; Lehmann, U.; Seekamp, A. Prehospital care, importance of early intervention on outcome. *Acta Anaesthesiologica Scandinavica* **1997**, *41* (S110), 71−76.
(5) Cannon, J. W. Hemorrhagic Shock. *N Engl J. Med.* **2018**, *378* (4), 370−379.
(6) Cap, A. P.; Cannon, J. W.; Reade, M. C. Synthetic blood and blood products for combat casualty care and beyond. *J. Trauma Acute Care Surg* **2021**, *91* (2S Suppl 2), S26−S32.
(7) Anselmo, A. C.; Modery-Pawlowski, C. L.; Menegatti, S.; Kumar, S.; Vogus, D. R.; Tian, L. L.; Chen, M.; Squires, T. M.; Sen Gupta, A.; Mitragotri, S. Platelet-like nanoparticles: mimicking shape, flexibility, and surface biology of platelets to target vascular injuries. *ACS Nano* **2014**, *8* (11), 11243−53.
(8) Baylis, J. R.; Yeon, J. H.; Thomson, M. H.; Kazerooni, A.; Wang, X.; St. John, A. E.; Lim, E. B.; Chien, D.; Lee, A.; Zhang, J. Q.; Piret, J. M.; Machan, L. S.; Burke, T. F.; White, N. J.; Kastrup, C. J. Self-propelled particles that transport cargo through flowing blood and halt hemorrhage. *Science advances* **2015**, *1* (9), e1500379.
(9) Gkikas, M.; Peponis, T.; Mesar, T.; Hong, C.; Avery, R. K.; Roussakis, E.; Yoo, H. J.; Parakh, A.; Patino, M.; Sahani, D. V.; Watkins, M. T.; Oklu, R.; Evans, C. L.; Albadawi, H.; Velmahos, G.; Olsen, B. D. Systemically Administered Hemostatic Nanoparticles for Identification and Treatment of Internal Bleeding. *ACS Biomater Sci. Eng.* **2019**, *5* (5), 2563−2576.
(10) Brown, A. C.; Stabenfeldt, S. E.; Ahn, B.; Hannan, R. T.; Dhada, K. S.; Herman, E. S.; Stefanelli, V.; Guzzetta, N.; Alexeev, A.; Lam, W. A.; Lyon, L. A.; Barker, T. H. Ultrasoft microgels displaying emergent platelet-like behaviours. *Nature materials* **2014**, *13* (12), 1108−1114.
(11) Fernandez-Moure, J.; Maisha, N.; Lavik, E. B.; Cannon, J. The chemistry of lyophilized blood products. *Bioconjug Chem.* **2018**, *29* (7), 2150−2160.
(12) Moghimi, S. M.; Wibroe, P. P.; Helvig, S. Y.; Farhangrazi, Z. S.; Hunter, A. C. Genomic perspectives in inter-individual adverse responses following nanomedicine administration: The way forward. *Adv. Drug Deliv Rev.* **2012**, *64* (13), 1385−93.
(13) Thasneem, Y. M.; Sajeesh, S.; Sharma, C. P. Glucosylated polymeric nanoparticles: a sweetened approach against blood compatibility paradox. *Colloids Surf. B Biointerfaces* **2013**, *108*, 337−44.
(14) Rampton, D.; Folkersen, J.; Fishbane, S.; Hedenus, M.; Howaldt, S.; Locatelli, F.; Patni, S.; Szebeni, J.; Weiss, G. Hypersensitivity reactions to intravenous iron: guidance for risk minimization and management. *Haematologica* **2014**, *99* (11), 1671−6.
(15) Fornaguera, C.; Caldero, G.; Mitjans, M.; Vinardell, M. P.; Solans, C.; Vauthier, C. Interactions of PLGA nanoparticles with blood components: protein adsorption, coagulation, activation of the complement system and hemolysis studies. *Nanoscale* **2015**, *7* (14), 6045−58.
(16) Li, Y.; Fung, J.; Lin, F. Local Inhibition of Complement Improves Mesenchymal Stem Cell Viability and Function After Administration. *Mol. Ther* **2016**, *24* (9), 1665−74.
(17) Goram, A. L.; Richmond, P. L. Pegylated liposomal doxorubicin: tolerability and toxicity. *Pharmacotherapy* **2001**, *21* (6), 751−63.
(18) Janssen, B. J.; Huizinga, E. G.; Raaijmakers, H. C.; Roos, A.; Daha, M. R.; Nilsson-Ekdahl, K.; Nilsson, B.; Gros, P. Structures of complement component C3 provide insights into the function and evolution of immunity. *Nature* **2005**, *437* (7058), 505−11.
(19) Dawson, K.; Moran, M.; Guindon, K.; Wan, H. Managing Infusion-Related Reactions for Patients With Chronic Lymphocytic Leukemia Receiving Obinutuzumab. *Clin J. Oncol Nurs* **2016**, *20* (2), E41−8.
(20) Fulop, T.; Kozma, G. T.; Vashegyi, I.; Meszaros, T.; Rosivall, L.; Urbanics, R.; Storm, G.; Metselaar, J. M.; Szebeni, J. Liposome-induced hypersensitivity reactions: Risk reduction by design of safe infusion protocols in pigs. *J. Controlled Release* **2019**, *309*, 333−338.
(21) Lashof-Sullivan, M.; Holland, M.; Groynom, R.; Campbell, D.; Shoffstall, A.; Lavik, E. Hemostatic Nanoparticles Improve Survival Following Blunt Trauma Even after 1 Week Incubation at 50 (degrees)C. *ACS Biomater Sci. Eng.* **2016**, *2* (3), 385−392.
(22) Hubbard, W. B.; Lashof-Sullivan, M. M.; Lavik, E. B.; VandeVord, P. J. Steroid-Loaded Hemostatic Nanoparticles Combat Lung Injury after Blast Trauma. *ACS Macro Lett.* **2015**, *4* (4), 387−391.
(23) Lashof-Sullivan, M. M.; Shoffstall, E.; Atkins, K. T.; Keane, N.; Bir, C.; VandeVord, P.; Lavik, E. B. Intravenously administered nanoparticles increase survival following blast trauma. *Proc. Natl. Acad. Sci. U. S. A.* **2014**, *111* (28), 10293−8.
(24) Shoffstall, A. J.; Everhart, L. M.; Varley, M. E.; Soehnlen, E. S.; Shick, A. M.; Ustin, J. S.; Lavik, E. B. Tuning ligand density on intravenous hemostatic nanoparticles dramatically increases survival following blunt trauma. *Biomacromolecules* **2013**, *14* (8), 2790−7.
(25) Shoffstall, A. J.; Atkins, K. T.; Groynom, R. E.; Varley, M. E.; Everhart, L. M.; Lashof-Sullivan, M. M.; Martyn-Dow, B.; Butler, R. S.; Ustin, J. S.; Lavik, E. B. Intravenous hemostatic nanoparticles increase survival following blunt trauma injury. *Biomacromolecules* **2012**, *13* (11), 3850−7.
(26) Onwukwe, C.; Maisha, N.; Holland, M.; Varley, M.; Groynom, R.; Hickman, D.; Uppal, N.; Shoffstall, A.; Ustin, J.; Lavik, E. Engineering Intravenously Administered Nanoparticles to Reduce Infusion Reaction and Stop Bleeding in a Large Animal Model of Trauma. *Bioconjug Chem.* **2018**, *29* (7), 2436−2447.
(27) Maisha, N.; Coombs, T.; Lavik, E. Development of a Sensitive Assay to Screen Nanoparticles in vitro for Complement Activation. *ACS Biomater Sci. Eng.* **2020**, *6* (9), 4903−4915.
(28) Maisha, N.; Naik, N.; Okesola, M.; Coombs, T.; Zilberberg, R.; Pandala, N.; Lavik, E. Engineering PEGylated Polyester Nanoparticles to Reduce Complement-Mediated Infusion Reaction. *Bioconjugate Chem.* **2021**, *32*, 2154.
(29) Gurney, J.; Philbin, N.; Rice, J.; Arnaud, F.; Dong, F.; Wulster-Radcliffe, M.; Pearce, L. B.; Kaplan, L.; McCarron, R.; Freilich, D. A Hemoglobin Based Oxygen Carrier, Bovine Polymerized Hemoglobin (HBOC-201) versus Hetastarch (HEX) in an Uncontrolled Liver Injury Hemorrhagic Shock Swine Model with Delayed Evacuation. *Journal of Trauma: Injury, Infection, and Critical Care* **2004**, *57*, 726−738.
(30) Jackson, M. A.; Patel, S. S.; Yu, F.; Cottam, M. A.; Glass, E. B.; Hoogenboezem, E. N.; Fletcher, R. B.; Dollinger, B. R.; Patil, P.; Liu, D. D.; Kelly, I. B.; Bedingfield, S. K.; King, A. R.; Miles, R. E.; Hasty, A. M.; Giorgio, T. D.; Duvall, C. L. Kupffer cell release of platelet activating factor drives dose limiting toxicities of nucleic acid nanocarriers. *Biomaterials* **2021**, *268*, 120528.
(31) Bertram, J. P.; Williams, C. A.; Robinson, R.; Segal, S. S.; Flynn, N. T.; Lavik, E. B. Intravenous hemostat: nanotechnology to halt bleeding. *Sci. Transl Med.* **2009**, *1* (11), 11ra22.

https://doi.org/10.1021/acsnano.2c01993
ACS Nano 2022, 16, 10566−10580

(32) Sapkota, B.; Shrestha, S. K.; Poudel, S. Association of activated partial thromboplastin time and fibrinogen level in patients with type II diabetes mellitus. *BMC research notes* **2013**, *6*, 485.
(33) Esmon, C. T. Possible involvement of cytokines in diffuse intravascular coagulation and thrombosis. *Bailliere's best practice & research. Clinical haematology* **1999**, *12* (3), 343−59.
(34) Grignani, G.; Maiolo, A. Cytokines and hemostasis. *Haematologica* **2000**, *85* (9), 967−972.
(35) Stouthard, J. M.; Levi, M.; Hack, C. E.; Veenhof, C. H.; Romijn, H. A.; Sauerwein, H. P.; van der Poll, T. Interleukin-6 stimulates coagulation, not fibrinolysis, in humans. *Thromb Haemost* **1996**, *76* (5), 738−742.
(36) Eslamifar, Z.; Behzadifard, M.; Soleimani, M.; Behzadifard, S. Coagulation abnormalities in SARS-CoV-2 infection: overexpression tissue factor. *Thrombosis journal* **2020**, *18* (1), 38.
(37) Faille, D.; Lamrani, L.; Loyau, S.; Huisse, M. G.; Bourrienne, M. C.; Alkhaier, S.; Cassinat, B.; Boulaftali, Y.; Debus, J.; Jandrot-Perrus, M.; Chomienne, C.; Dosquet, C.; Ajzenberg, N. Interferon Alpha Therapy Increases Pro-Thrombotic Biomarkers in Patients with Myeloproliferative Neoplasms. *Cancers (Basel)* **2020**, *12* (4), 992.
(38) Focosi, D.; Franchini, M.; Pirofski, L. A.; Burnouf, T.; Fairweather, D.; Joyner, M. J.; Casadevall, A. COVID-19 Convalescent Plasma Is More than Neutralizing Antibodies: A Narrative Review of Potential Beneficial and Detrimental Co-Factors. *Viruses* **2021**, *13* (8), 1594.
(39) Chen, Y.; Wang, J.; Liu, C.; Su, L.; Zhang, D.; Fan, J.; Yang, Y.; Xiao, M.; Xie, J.; Xu, Y.; Li, Y.; Zhang, S. IP-10 and MCP-1 as biomarkers associated with disease severity of COVID-19. *Mol. Med.* **2020**, *26* (1), 97.
(40) Han, Y.; He, T.; Huang, D. R.; Pardo, C. A.; Ransohoff, R. M. TNF-alpha mediates SDF-1 alpha-induced NF-kappa B activation and cytotoxic effects in primary astrocytes. *J. Clin Invest* **2001**, *108* (3), 425−35.
(41) Yates, A. G.; Jogia, T.; Gillespie, E. R.; Couch, Y.; Ruitenberg, M. J.; Anthony, D. C. Acute IL-1RA treatment suppresses the peripheral and central inflammatory response to spinal cord injury. *J. Neuroinflammation* **2021**, *18* (1), 15.
(42) Arend, W. P. The balance between IL-1 and IL-1Ra in disease. *Cytokine Growth Factor Rev.* **2002**, *13* (4−5), 323−40.
(43) Roth, S.; Agthe, M.; Eickhoff, S.; Möller, S.; Karsten, C. M.; Borregaard, N.; Solbach, W.; Laskay, T. Secondary necrotic neutrophils release interleukin-16C and macrophage migration inhibitory factor from stores in the cytosol. *Cell Death Discovery* **2015**, *1*, 15056.
(44) Cruikshank, W. W.; Kornfeld, H.; Center, D. M. Interleukin-16. *Journal of leukocyte biology* **2000**, *67* (6), 757−66.
(45) Mathy, N. L.; Scheuer, W.; Lanzendörfer, M.; Honold, K.; Ambrosius, D.; Norley, S.; Kurth, R. Interleukin-16 stimulates the expression and production of pro-inflammatory cytokines by human monocytes. *Immunology* **2000**, *100* (1), 63−9.
(46) Gerhard, R.; Queisser, S.; Tatge, H.; Meyer, G.; Dittrich-Breiholz, O.; Kracht, M.; Feng, H.; Just, I. Down-regulation of interleukin-16 in human mast cells HMC-1 by Clostridium difficile toxins A and B. *Naunyn Schmiedebergs Arch Pharmacol* **2011**, *383* (3), 285−95.
(47) Schindler, L.; Smyth, L. C. D.; Bernhagen, J.; Hampton, M. B.; Dickerhof, N. Macrophage migration inhibitory factor (MIF) enhances hypochlorous acid production in phagocytic neutrophils. *Redox biology* **2021**, *41*, 101946.
(48) Barrett, C D; Hsu, A T; Ellson, C D; Miyazawa, B Y; Kong, Y-W; Greenwood, J D; Dhara, S; Neal, M D; Sperry, J L; Park, M S; Cohen, M J; Zuckerbraun, B S; Yaffe, M B Blood clotting and traumatic injury with shock mediates complement-dependent neutrophil priming for extracellular ROS, ROS-dependent organ injury and coagulopathy. *Clinical and experimental immunology* **2018**, *194* (1), 103−117.
(49) Peralta, R.; Thani, H. A.; Rizoli, S. Coagulopathy in the surgical patient: trauma-induced and drug-induced coagulopathies. *Curr. Opin Crit Care* **2019**, *25* (6), 668−674.
(50) Moore, E. E.; Moore, H. B.; Kornblith, L. Z.; Neal, M. D.; Hoffman, M.; Mutch, N. J.; Schöchl, H.; Hunt, B. J.; Sauaia, A. Trauma-induced coagulopathy. *Nat. Rev. Dis. Primers* **2021**, *7* (1), 30.
(51) Baylis, J. R.; Chan, K. Y.; Kastrup, C. J. Halting hemorrhage with self-propelling particles and local drug delivery. *Thromb Res.* **2016**, *141* (Suppl 2), S36−S39.
(52) Hubbard, W. B.; Lashof-Sullivan, M.; Greenberg, S.; Norris, C.; Eck, J.; Lavik, E.; VandeVord, P. Hemostatic nanoparticles increase survival, mitigate neuropathology and alleviate anxiety in a rodent blast trauma model. *Sci. Rep.* **2018**, *8* (1), 10622.
(53) Luo, T.; Hao, S.; Chen, X.; Wang, J.; Yang, Q.; Wang, Y.; Weng, Y.; Wei, H.; Zhou, J.; Wang, B. Development and assessment of kerateine nanoparticles for use as a hemostatic agent. *Materials science & engineering. C, Materials for biological applications* **2016**, *63*, 352−8.
(54) Okamura, Y.; Takeoka, S.; Eto, K.; Maekawa, I.; Fujie, T.; Maruyama, H.; Ikeda, Y.; Handa, M. Development of fibrinogen γ-chain peptide-coated, adenosine diphosphate-encapsulated liposomes as a synthetic platelet substitute. *Journal of Thrombosis and Haemostasis* **2009**, *7*, 470−477.
(55) Jackman, J. A.; Meszaros, T.; Fulop, T.; Urbanics, R.; Szebeni, J.; Cho, N. J. Comparison of complement activation-related pseudoallergy in miniature and domestic pigs: foundation of a validatable immune toxicity model. *Nanomedicine* **2016**, *12* (4), 933−943.
(56) Szebeni, J. Mechanism of nanoparticle-induced hypersensitivity in pigs: complement or not complement? *Drug Discov Today* **2018**, *23* (3), 487−492.
(57) Brown, D.; Namas, R. A.; Almahmoud, K.; Zaaqoq, A.; Sarkar, J.; Barclay, D. A.; Yin, J.; Ghuma, A.; Abboud, A.; Constantine, G.; Nieman, G.; Zamora, R.; Chang, S. C.; Billiar, T. R.; Vodovotz, Y. Trauma in silico: Individual-specific mathematical models and virtual clinical populations. *Sci. Transl. Med.* **2015**, *7* (285), 285ra61.
(58) Fromen, C. A.; Kelley, W. J.; Fish, M. B.; Adili, R.; Noble, J.; Hoenerhoff, M. J.; Holinstat, M.; Eniola-Adefeso, O. Neutrophil-Particle Interactions in Blood Circulation Drive Particle Clearance and Alter Neutrophil Responses in Acute Inflammation. *ACS Nano* **2017**, *11* (11), 10797−10807.
(59) Chatfield, S. M.; Thieblemont, N.; Witko-Sarsat, V. Expanding Neutrophil Horizons: New Concepts in Inflammation. *J. Innate Immun* **2018**, *10* (5−6), 422−431.
(60) Kelley, W. J.; Fromen, C. A.; Lopez-Cazares, G.; Eniola-Adefeso, O. PEGylation of model drug carriers enhances phagocytosis by primary human neutrophils. *Acta Biomater* **2018**, *79*, 283−293.
(61) Kelley, W. J.; Onyskiw, P. J.; Fromen, C. A.; Eniola-Adefeso, O. Model Particulate Drug Carriers Modulate Leukocyte Adhesion in Human Blood Flows. *ACS Biomater Sci. Eng.* **2019**, *5* (12), 6530−6540.
(62) Zolnik, B. S.; González-Fernández, A.; Sadrieh, N.; Dobrovolskaia, M. A. Nanoparticles and the immune system. *Endocrinology* **2010**, *151* (2), 458−65.
(63) Ben-Akiva, E.; Est Witte, S.; Meyer, R. A.; Rhodes, K. R.; Green, J. J. Polymeric micro- and nanoparticles for immune modulation. *Biomaterials science* **2019**, *7* (1), 14−30.
(64) Ayer, M.; Burri, O.; Guiet, R.; Seitz, A.; Kaba, E.; Engelhardt, B.; Klok, H. A. Biotin-NeutrAvidin Mediated Immobilization of Polymer Micro- and Nanoparticles on T Lymphocytes. *Bioconjug Chem.* **2021**, *32* (3), 541−552.
(65) Ruf, W.; Ruggeri, Z. M. Neutrophils release brakes of coagulation. *Nat. Med.* **2010**, *16* (8), 851−2.
(66) Fu, J.; Kong, J.; Wang, W.; Wu, M.; Yao, L.; Wang, Z.; Jin, J.; Wu, D.; Yu, X. The clinical implication of dynamic neutrophil to lymphocyte ratio and D-dimer in COVID-19: A retrospective study in Suzhou China. *Thromb Res.* **2020**, *192*, 3−8.
(67) Terpos, E.; Ntanasis-Stathopoulos, I.; Elalamy, I.; Kastritis, E.; Sergentanis, T. N.; Politou, M.; Psaltopoulou, T.; Gerotziafas, G.; Dimopoulos, M. A. Hematological findings and complications of COVID-19. *American journal of hematology* **2020**, *95* (7), 834−847.

https://doi.org/10.1021/acsnano.2c01993
ACS Nano 2022, 16, 10566−10580

(68) Zhao, J.; Liu, K.; Li, S.; Gao, Y.; Zhao, L.; Liu, H.; Fang, H.; Song, B.; Xu, Y. Neutrophil-to-lymphocyte Ratio Predicts the Outcome of Cerebral Venous Thrombosis. *Curr. Neurovasc Res.* **2021**, *18* (2), 204−210.
(69) Moghimi, S. M. Nanomedicine safety in preclinical and clinical development: focus on idiosyncratic injection/infusion reactions. *Drug Discov Today* **2018**, *23* (5), 1034−1042.
(70) Skotland, T. Injection of nanoparticles into cloven-hoof animals: Asking for trouble. *Theranostics* **2017**, *7* (19), 4877−4878.
(71) Sondeen, J. L.; de Guzman, R.; Amy Polykratis, I.; Dale Prince, M.; Hernandez, O.; Cap, A. P.; Dubick, M. A. Comparison between human and porcine thromboelastograph parameters in response to ex-vivo changes to platelets, plasma, and red blood cells. *Blood Coagul Fibrinolysis* **2013**, *24* (8), 818−29.
(72) Tarandovskiy, I. D.; Shin, H. K. H.; Baek, J. H.; Karnaukhova, E.; Buehler, P. W. Interspecies comparison of simultaneous thrombin and plasmin generation. *Sci. Rep.* **2020**, *10* (1), 3885.
(73) Gando, S.; Levi, M.; Toh, C. H. Disseminated intravascular coagulation. *Nat. Rev. Dis. Primers* **2016**, *2*, 16037.
(74) Cardenas, J. C.; Wade, C. E.; Holcomb, J. B. Mechanisms of trauma-induced coagulopathy. *Curr. Opin Hematol* **2014**, *21* (5), 404−9.
(75) Innerhofer, P.; Fries, D.; Mittermayr, M.; Innerhofer, N.; von Langen, D.; Hell, T.; Gruber, G.; Schmid, S.; Friesenecker, B.; Lorenz, I. H.; Strohle, M.; Rastner, V.; Trubsbach, S.; Raab, H.; Treml, B.; Wally, D.; Treichl, B.; Mayr, A.; Kranewitter, C.; Oswald, E. Reversal of trauma-induced coagulopathy using first-line coagulation factor concentrates or fresh frozen plasma (RETIC): a single-centre, parallel-group, open-label, randomised trial. *Lancet. Haematology* **2017**, *4* (6), e258−e271.
(76) Samuels, J. M.; Moore, E. E.; Silliman, C. C.; Banerjee, A.; Cohen, M. J.; Ghasabyan, A.; Chandler, J.; Coleman, J. R.; Sauaia, A. Severe traumatic brain injury is associated with a unique coagulopathy phenotype. *J. Trauma Acute Care Surg* **2019**, *86* (4), 686−693.
(77) King, D. R.; Cohn, S. M.; Proctor, K. G. Changes in intracranial pressure, coagulation, and neurologic outcome after resuscitation from experimental traumatic brain injury with hetastarch. *Surgery* **2004**, *136* (2), 355−63.
(78) Kumar, M. A. Coagulopathy associated with traumatic brain injury. *Curr. Neurol. Neurosci. Rep.* **2013**, *13* (11), 391.
(79) Chang, R.; Cardenas, J. C.; Wade, C. E.; Holcomb, J. B. Advances in the understanding of trauma-induced coagulopathy. *Blood* **2016**, *128* (8), 1043−9.
(80) Hess, J. R.; Brohi, K.; Dutton, R. P.; Hauser, C. J.; Holcomb, J. B.; Kluger, Y.; Mackway-Jones, K.; Parr, M. J.; Rizoli, S. B.; Yukioka, T.; et al. The coagulopathy of trauma: a review of mechanisms. *Journal of Trauma-Injury, Infection, and Critical Care* **2008**, *65* (4), 748−754.
(81) Bajzar, L.; Jain, N.; Wang, P.; Walker, J. B. Thrombin activatable fibrinolysis inhibitor: not just an inhibitor of fibrinolysis. *Crit Care Med.* **2004**, *32* (5 Suppl), S320−S324.
(82) Brohi, K.; Cohen, M. J.; Davenport, R. A. Acute coagulopathy of trauma: mechanism, identification and effect. *Curr. Opin Crit Care* **2007**, *13* (6), 680−5.
(83) Spahn, D. R.; Bouillon, B.; Cerny, V.; Coats, T. J.; Duranteau, J.; Fernandez-Mondejar, E.; Filipescu, D.; Hunt, B. J.; Komadina, R.; Nardi, G.; Neugebauer, E.; Ozier, Y.; Riddez, L.; Schultz, A.; Vincent, J. L.; Rossaint, R. Management of bleeding and coagulopathy following major trauma: an updated European guideline. *Crit Care* **2013**, *17* (2), R76.
(84) Rossaint, R.; Bouillon, B.; Cerny, V.; Coats, T. J.; Duranteau, J.; Fernandez-Mondejar, E.; Filipescu, D.; Hunt, B. J.; Komadina, R.; Nardi, G.; Neugebauer, E. A.; Ozier, Y.; Riddez, L.; Schultz, A.; Vincent, J. L.; Spahn, D. R. The European guideline on management of major bleeding and coagulopathy following trauma: fourth edition. *Crit. Care* **2016**, *20*, 100.
(85) Sumislawski, J. J.; Kornblith, L. Z.; Conroy, A. S.; Callcut, R. A.; Cohen, M. J. Dynamic coagulability after injury: Is delaying venous thromboembolism chemoprophylaxis worth the wait? *J. Trauma Acute Care Surg* **2018**, *85* (5), 907−914.
(86) Antovic, A. Screening haemostasis–looking for global assays: the Overall Haemostasis Potential (OHP) method–a possible tool for laboratory investigation of global haemostasis in both hypo- and hypercoagulable conditions. *Current vascular pharmacology* **2008**, *6* (3), 173−85.
(87) Duque, P.; Mora, L.; Levy, J. H.; Schöchl, H. Pathophysiological Response to Trauma-Induced Coagulopathy: A Comprehensive Review. *Anesth Analg* **2020**, *130* (3), 654−664.
(88) Ma, X.; Cheng, Y.; Garcia, R.; Haorah, J. Hemorrhage Associated Mechanisms of Neuroinflammation in Experimental Traumatic Brain Injury. *J. Neuroimmune Pharmacol* **2020**, *15* (2), 181−195.
(89) McMillan, T. M.; Teasdale, G. M. Death rate is increased for at least 7 years after head injury: a prospective study. *Brain* **2007**, *130* (Pt 10), 2520−7.
(90) Ma, X.; Aravind, A.; Pfister, B. J.; Chandra, N.; Haorah, J. Animal Models of Traumatic Brain Injury and Assessment of Injury Severity. *Mol. Neurobiol* **2019**, *56* (8), 5332−5345.
(91) Cannon, J. W.; Dias, J. D.; Kumar, M. A.; Walsh, M.; Thomas, S. G.; Cotton, B. A.; Schuster, J. M.; Evans, S. L.; Schreiber, M. A.; Adam, E. H.; Zacharowski, K.; Hartmann, J.; Schöchl, H.; Kaplan, L. J. Use of Thromboelastography in the Evaluation and Management of Patients With Traumatic Brain Injury: A Systematic Review and Meta-Analysis. *Crit Care Explor* **2021**, *3* (9), e0526.
(92) Esnault, P.; Mathais, Q.; D'Aranda, E.; Montcriol, A.; Cardinale, M.; Cungi, P. J.; Goutorbe, P.; Joubert, C.; Dagain, A.; Meaudre, E. Ability of Fibrin Monomers to Predict Progressive Hemorrhagic Injury in Patients with Severe Traumatic Brain Injury. *Neurocrit Care* **2020**, *33* (1), 182−195.
(93) Tur Martínez, J.; Petrone, P.; Axelrad, A.; Marini, C. P. Comparison between thromboelastography and conventional coagulation test: Should we abandon conventional coagulation tests in polytrauma patients? *Cirugia espanola* **2018**, *96* (7), 443−449.
(94) Tian, Y.; Salsbery, B.; Wang, M.; Yuan, H.; Yang, J.; Zhao, Z.; Wu, X.; Zhang, Y.; Konkle, B. A.; Thiagarajan, P.; Li, M.; Zhang, J.; Dong, J. F. Brain-derived microparticles induce systemic coagulation in a murine model of traumatic brain injury. *Blood* **2015**, *125* (13), 2151−9.
(95) Ackermann, M.; Verleden, S. E.; Kuehnel, M.; Haverich, A.; Welte, T.; Laenger, F.; Vanstapel, A.; Werlein, C.; Stark, H.; Tzankov, A.; Li, W. W.; Li, V. W.; Mentzer, S. J.; Jonigk, D. Pulmonary Vascular Endothelialitis, Thrombosis, and Angiogenesis in Covid-19. *N Engl J. Med.* **2020**, *383* (2), 120−128.
(96) Fogarty, H.; Townsend, L.; Morrin, H.; Ahmad, A.; Comerford, C.; Karampini, E.; Englert, H.; Byrne, M.; Bergin, C.; O'Sullivan, J. M.; Martin-Loeches, I.; Nadarajan, P.; Bannan, C.; Mallon, P. W.; Curley, G. F.; Preston, R. J. S.; Rehill, A. M.; McGonagle, D.; Ni Cheallaigh, C.; Baker, R. I.; Renné, T.; Ward, S. E.; O'Donnell, J. S. Persistent endotheliopathy in the pathogenesis of long COVID syndrome. *J. Thromb. Haemost.* **2021**, *19* (10), 2546−2553.
(97) Iba, T.; Connors, J. M.; Levy, J. H. The coagulopathy, endotheliopathy, and vasculitis of COVID-19. *Inflamm. Res.* **2020**, *69* (12), 1181−1189.
(98) Connor, E. F.; Nyce, G. W.; Myers, M.; Möck, A.; Hedrick, J. L. First Example of N-Heterocyclic Carbenes as Catalysts for Living Polymerization: Organocatalytic Ring-Opening Polymerization of Cyclic Esters. *J. Am. Chem. Soc.* **2002**, *124*, 914−915.
(99) Philbin, N.; Rice, J.; Gurney, J.; McGwin, G.; Arnaud, F.; Dong, F.; Johnson, T.; Flournoy, W. S.; Ahlers, S.; Pearce, L. B.; McCarron, R.; Freilich, D. A hemoglobin-based oxygen carrier, bovine polymerized hemoglobin (HBOC-201) versus hetastarch (HEX) in a moderate severity hemorrhagic shock swine model with delayed evacuation. *Resuscitation* **2005**, *66*, 367−378.
(100) Lategan, K.; Alghadi, H.; Bayati, M.; de Cortalezzi, M. F.; Pool, E. Effects of Graphene Oxide Nanoparticles on the Immune System Biomarkers Produced by RAW 264.7 and Human Whole

https://doi.org/10.1021/acsnano.2c01993
ACS Nano 2022, 16, 10566−10580

Blood Cell Cultures. *Nanomaterials (Basel, Switzerland)* **2018**, *8* (2), 125.

https://doi.org/10.1021/acsnano.2c01993
ACS Nano 2022, 16, 10566−10580